Two-step processed efficient perovskite solar cells via improving perovskite/PTAA interface using solvent engineering in PbI_2 precursor*

Cao-Yu Long(龙操玉)†, Ning Wang(王宁)†, Ke-Qing Huang(黄可卿)†, Heng-Yue Li(李恒月), Biao Liu(刘标), and Jun-Liang Yang(阳军亮)‡

Hunan Key Laboratory for Super-microstructure and Ultrafast Process, School of Physics and Electronics, Central South University, Changsha 410083, *China*

(Received 10 January 2020; revised manuscript received 23 January 2020; accepted manuscript online 18 February 2020)

The morphology and interface of perovskite film are very important for the performance of perovskite solar cells (PSCs). The quality of perovskite film, fabricated via two-step spin-coating process, is significantly influenced by the morphology and crystallinity of PbI_2 film. With the addition of additive dimethyl sulfoxide (DMSO) into the PbI_2 precursor, the roughness and trap-state density of perovskite film have been significantly reduced, leading to the excellent contact between perovskite layer and subsequent deposited carrier transport layer. Accordingly, the planar heterojunction PSCs with an architecture of ITO/SnO_2/perovskite/PTAA/Ag show an efficiency up to 19.02%. Furthermore, PSCs exhibit promising stability in air with a humidity of $\sim$ 45%, and retain 80% of initial efficiency after being exposed to air for 400 h without any encapsulation.

Keywords: perovskite solar cells, planar heterojunction, interface, PbI_2-DMSO complex

PACS: 88.40.H–, 88.40.hj, 88.40.ff **DOI:** 10.1088/1674-1056/ab7744

1. Introduction

Perovskite solar cells (PSCs) have attracted much attention due to their spectacular breakthroughs in the past ten years, ascribed to the brilliant photovoltaic properties of perovskite materials[1–4] and modification of alternative functional layers.[5,6] Up to now, the certified power conversion efficiency (PCE) has been enhanced to 25.2%,[7] reflecting the promising commercial applications of PSCs. The PCE of PSCs relies on efficient charge carrier extraction at interfaces.[8] The quality of perovskite layer and the properties of charge transport layers, *i.e.*, hole transport layer (HTL) and electron transport layer (ETL), are the two key factors that affect the interfacial contact, especially the HTL in PSCs with n–i–p configuration. Poly[bis(4-phenyl)(2,4,6-trimethylphenyl)amine] (PTAA) is a stable p-type polymer with high hole mobility and suitable energy level. Thus, it has been used as the HTL in PSCs since the early stage in the development of PSCs because of its prominent transport ability.[9] In fact, considerably high PCE of 22.1% was achieved for PSCs with PTAA as the HTL.[10] However, the interfacial contact between perovskite and PTAA is a thorny problem in n–i–p structural PSCs due to the hydrophobic property of PTAA.

A lot of strategies have been suggested to improve the interfacial contact between the perovskite and PTAA. Solvent engineering assisted one-step solution deposition was introduced to achieve PTAA-based PSCs with a PCE of 16.2%.[11] The high fill factor (FF) over 75% was achieved in this device, which is ascribed to the exquisite interface contact between $MAPbI_3$ and PTAA derived from the modification of perovskite grain and surface. Meanwhile, PTAA-based graded heterojunction was achieved for good interface between perovskite and HTL by involving PTAA in the anti-solvent, one-step solution deposited perovskite.[12]

Two-step sequential deposition has been widely used to fabricate perovskite film and accordingly produce efficient PSCs.[13–17] Nevertheless, because of the complexion of reaction, it is still difficult to control the nucleation and growth of perovskite crystal. Thus, the perovskite film often shows incomplete conversion and poor surface roughness,[18,19] which are disadvantageous to the stability and the interfacial contact between perovskite and other functional layers. It was reported that the large molecular mass of PTAA induces a rough contact between PTAA and perovskite, leading the performance of PSC with n–i–p architecture to degenerate.[20] Several methods have been proposed to modify the perovskite films via two-step sequential process by controlling PbI_2 film through manipulating the PbI_2 precursor, including adding water,[21] PCBM,[22] 1,8-diiodooctane (DOI),[23] hydroiodic acid (HI),[24] hydrochloric acid (HCl),[25] *etc*.

Here in this work, PTAA as the HTL is introduced to fabricate planar heterojunction (PHJ) PSCs with n–i–p architec-

*Project supported by the National Natural Science Foundation of China (Grant No. 51673214) and the National Key Research and Development Program of China (Grant No. 2017YFA0206600).

†These authors contributed equally to this work.

‡Corresponding author. E-mail: junliang.yang@csu.edu.cn

ture. The active layer perovskite composed of triple cations $CH_3NH_3^+(MA^+)$, $HC(NH_2)_2^+(FA^+)$, and Cs^+ is produced by the reproducible and low-temperature two-step sequential deposition. By optimizing the ratio of dimethyl sulfoxide (DMSO) to N,N-dimethylformamide (DMF) in PbI_2 precursor, a delicate, high-quality PbI_2 with appropriate crystallinity and porosity is formed. Furthermore, a modified interface between perovskite and PTAA with better stability is achieved by post-annealing PbI_2-DMSO complex. The PSC with a simple structure of ITO/SnO_2/perovskite/PTAA/Ag shows a PCE with up to 19.02%. The study is helpful in understanding the interface contact between perovskite and PTAA in PHJ PSCs with n–i–p architecture and promotes the scaled up utilization of PTAA in the fabrication of potential large-scaled PSCs.

2. Experiment

2.1. Materials

The materials were purchased without further purification, including: $NH_2CH{=}NH_2I$ (FAI) (99.5%, Xi'an Polymer Light Technology Corp.), CH_3NH_2Br (MABr) (99.5%, Xi'an Polymer Light Technology Corp.), CH_3NH_2Cl (MACl) (99.5%, Xi'an Polymer Light Technology Corp.), CsI (99%, Strem Chemicals, Inc.), PbI_2 (99%, Tianjing Weiyi Chemical Technology Co., Ltd), SnO_2 (15% in H_2O colloidal dispersion,Alfa Aesar), PTAA ($M_w = 33500$ g/mol, Xi'an Polymer Light Technology Corp.), Spiro-OMeTAD (99%, Wuhan Zhuojia Technology Co., Ltd), isopropanol (IPA) (99.5%, J & K Scientific), DMF (99.8%, Sigma-Aldrich), DMSO (99.8%, Sigma-Aldrich), chlorobenzene (CB) (99.8%, Sigma-Aldrich), and acetonitrile (99.95%, Sigma-Aldrich).

2.2. Methods

The patterned ITO was washed by acetone, deionized water, deionized water with detergent, IPA in an ultrasonic cleaner for 20 min, in sequence, followed by UV-ozone treatment for 25 min. The SnO_2 colloidal dispersion (with diluted concentration of 2.67%) was spin-coated onto ITO/glass substrate at 3000 rpm for 30 s. Then the film was annealed at 150 °C for 30 min. In the process of two-step sequential deposition of perovskite film, PbI_2 precursor solutions were prepared by dissolving 599.3 mg PbI_2 and 35 mg CsI in 1 mL DMF and DMSO mixed solvent with 4 types of volume mixing ratios (DMF : DMSO = 10 : 0, 9.5 : 0.5, 9 : 1, 8 : 2, which were named DMSO-0%, DMSO-5%, DMSO-10%, DMSO-20%, respectively) and were stirred at 75 °C overnight. The PbI_2 film was obtained by spin-coating PbI_2 precursor onto SnO_2-coated substrate at 1500 rpm for 30 s, followed by being annealed at 70 °C for 30 min. Then, FAI:MABr:MACl mixed solution (60 mg:6 mg:6 mg in 1 mL IPA) was spin-coated at 1500 rpm for 30 s. The perovskite film could be formed by heating the as-prepared film at 150 °C for 20 min under ambient conditions with a relative humidity of about 40%. The HTL was deposited by spin-coating PTAA solution with 12.5 mg PTAA dissolving in 1 mL toluene with an additive of 9.4 μL Li-TFSI solution (170 mg Li-TFSI in 1 mL acetonitrile) and 5 μL TBP at 3000 rpm for 30 s. For the Spiro-OMeTAD HTL, Spiro-OMeTAD solution prepared by dissolving 90 mg Spiro-OMeTAD, 45 μL Li-TFSI solution (170 mg Li-TFSI in 1 mL acetonitrile), and 10 μL TBP in 1 mL chlorobenzene, was deposited with the same spin-coating parameter as the PTAA HTL. Finally, the Ag electrode was deposited by thermal evaporation with a fixed area of 0.09 cm^2 through using metal mask. For evaluating the trap densities of perovskite, electron-only devices were created. The PCBM solution could be obtained by dissolving 20 mg PCBM into 1 mL chlorobenzene and stirring at 75 °C overnight. The spin-coating parameter of PCBM ETL was fixed at 3000 rpm for 30 s, without annealing process after being spin-coated.

2.3. Characterization

The absorbance spectra and crystallographic properties of PbI_2 and perovskite films were obtained by ultraviolet-visible spectrophotometer (UV-vis, Puxi, T9, China), x-ray diffractometer (XRD, Rigaku D, Max 2500, Japan), respectively. The morphology of PbI_2 and perovskite films were revealed by scanning electron microscope (SEM, FEI Helios Nanolab 600i SEM, America) and atomic force microscope (AFM, Agilent Technologies 5500AFM/SPM System), respectively, and the element composition of PbI_2 film was measured by the energy dispersive spectrometer (EDS). A digital source meter (Keithley, model 2420) was employed to measure the photovoltaic performance of as-prepared PSCs, with a scanning range from +1.2 V to −0.2 V, a 50-ms scanning delay, and 100 points in both reverse- and forward-scan modes, under a xenon-lamp-based solar simulator (Newport 91160 s, AM 1.5 G), whose light intensity of 100 mW/cm^2 had been calibrated by a standard silicon solar cell. To obtain the *I–V* curves of electron-only devices, the corresponding devices were measured under dark condition by a digital source meter, with increasing voltage from 0 V to 1.5 V applied and varied current recorded. The stability measurement was carried out under the *J–V* measurement condition and the statistics under forward-scan mode were recorded, after that the devices were stored under dark condition with a humidity of $\sim 40\%$.

3. Results and discussion

The PbI_2 precursors are made with the different solvents, *i.e.*, DMF : DMSO = 10:0, 9.5:0.5, 9:1, 8:2, which are named

DMSO-0%, DMSO-5%, DMSO-10%, DMSO-20%, respectively. In order to disclose how the additive DMSO influences the crystallization of PbI_2 film, the XRD experimental results of PbI_2 films are shown in Fig. 1(a). It is obvious that the intensity of diffraction peaks decreases with increasing the concentration of DMSO (Fig. 1(a)), indicating the gradual decrease in PbI_2 crystallinity. The crystallinity of PbI_2 film has a significant influence on the quality of subsequent perovskite film prepared by the two-step deposition. The PbI_2 with a low crystallinity will be helpful in completely converting the perovskite while the highly crystalline PbI_2 may contribute to controllable morphology and suitable excess PbI_2 content in final perovskite film.[26] Meanwhile, as shown in Fig. 1(b), it is obvious that the peak corresponding to the PbI_2(DMSO) complex appears and its intensity augments with increasing the concentration of DMSO.

The morphologies of PbI_2 films derived from the different solvents are revealed by SEM as illustrated in Figs. 2(a)–2(d). The morphology of PbI_2 film can be significantly affected by the DMSO concentration. The DMSO-0% PbI_2 film presents a loose, porous surface, with small-sized grains overlapping each other (Fig. 2(a)). The flake-like crystals and pores are found in DMSO-20% PbI_2 film (Fig. 2(d)). However, the DMSO-5% and DMSO-10% PbI_2 films are dense and uniform with smaller grains arranged compactly. Compared with the DMSO-5% PbI_2 film, the DMSO-10% PbI_2 film has many pores and crystallized particles on the surface. Furthermore, the PbI_2(DMSO) complex content in precursor film is detected by SEM–EDS analysis, and the results are shown in Fig. A1 and Fig. A2 in Appendix A. Atomic ratio (S) increasing with DMSO concentration rising is consistent with the XRD result.

The thermo-gravimetric analysis indicates that the PbI_2(DMSO) complex starts to decompose around 100 °C.[27] The PbI_2(DMSO) film post-annealed at 70 °C for 30 min contains little trace of PbI_2(DMSO) composite with the majority of DMSO molecules escaping from the system. The judgement can be also verified by no obvious shallow color

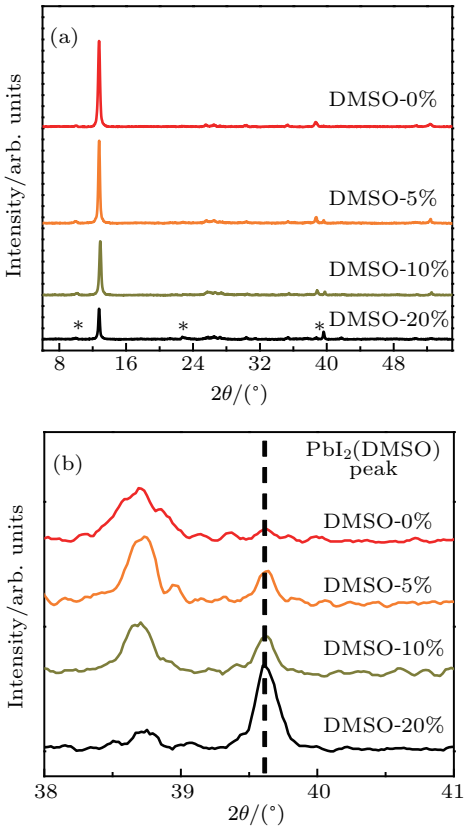

Fig. 1. (a) XRD patterns of PbI_2 derived from different solvents. Star marked peaks are ascribed to PbI_2 (DMSO) complex phase. (b) Magnified XRD patterns in region of 2θ from 38° to 41°.

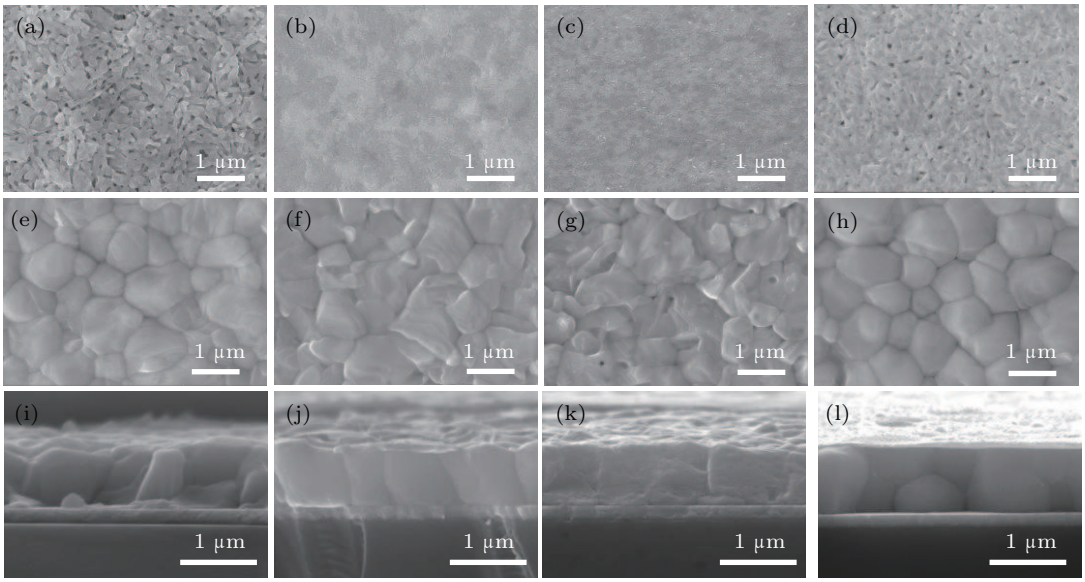

Fig. 2. SEM images of (a) DMSO-0%, (b) DMSO-5%, (c) DMSO-10%, and (d) DMSO-20% PbI_2 film, respectively. SEM images of perovskite films derived from (e) DMSO-0%, (f) DMSO-5%, (g) DMSO-10%, and (h) DMSO-20% PbI_2 precursor, respectively. Cross-section SEM images of perovskite films derived from (i) DMSO-0%, (j) DMSO-5%, (k) DMSO-10%, and (l) DMSO-20% PbI_2 precursor, respectively.

corresponding to FAI-DMSO-PbI_2 intermediate phase appearing in the second step of two-step deposition. The post-annealing treatment is speculated to account for this phenomenon, and the PbI_2-DMSO composite just exists in an intermediate. Therefore, the DMSO mainly affects the growth and morphology evolution of PbI_2 film. The little trace of PbI_2(DMSO) complex in the as-prepared PbI_2 film has light influence on the subsequent reaction.

The morphology evolution of PbI_2 film can be explained by the conversion of PbI_2(DMSO) complex in DMF solvent to PbI_2(DMSO) intermediate in wet film, and finally to the as-prepared precursor film after DMSO molecule escaping. In the case of DMSO-0%, the PbI_2 coordinates with DMF, forming one-dimensional structure along the *a* axis.[28] During PbI_2 film annealing, the DMF volatilizes from the wet film quickly and dendrite-like crystals tend to appear along the *a* axis. When the DMSO is incorporated, micella-shaped PbI_2(DMSO) complex forms with a certain concentration dispersed into DMF uniformly. It has been verified that the DMSO can inhibit the crystallization of PbI_2 when PbI_2 coordinates with DMSO molecule.[29] Therefore, the final precursor films derived from DMSO-5% and DMSO-10% show sphere-shaped grains with dense, flat morphology. With the DMSO increasing to 20%, the PbI_2(DMSO) complex is accumulated and the intermediate tend to be $PbI_2(DMSO)_2$,[26] which causes the macroscopic needle-like microcrystal to appear in solvent. After being annealed, the flake-like PbI_2 grains originating from the needle-like intermediate appears with DMSO molecule escaping and the remaining DMSO is coordinated with PbI_2 to form the PbI_2(DMSO) complex, which has been proved by the XRD analysis.

High-quality PbI_2 layer can play an important role in the subsequently depositing the perovskite layer in two-step spin-coating process. Figures 2(e)–2(h) and 2(i)–2(l) are the top view and cross section SEM images of perovskite films, respectively. The grain size in the perovskite films fabricated from DMSO-0%, DMSO-5%, DMSO-10%, and DMSO-20% PbI_2 films are shown in Fig. A3 and Table A1. Generally speaking, there is not uniform conclusion for the effect of DMSO on the grain size of perovskite film.[28,30] In our case, the results suggest that the grain sizes of perovskite films fabricated from DMSO-0%, DMSO-5%, DMSO-10%, and DMSO-20% PbI_2 films show the similar values, although perovskite film fabricated from DMSO-5% PbI_2 film shows a little bigger grain size. These size differences are in the range of statistical error. One may notice that in the case of DMSO-10%, some pin-holes can be found on the surface of grains (Fig. 2(g)), which may leave vacant place after the deposition of HTL. Moreover, in the case of DMSO-20%, loose contact between grains can be revealed in both top view and cross section images (Figs. 2(h) and 2(l)), resulting in large gaps between adjacent grains. In the case of DMSO-5%, vertically and tightly contacted grains demonstrate the high quality of perovskite film.

The perovskite films are characterized by XRD and shown in Fig. 3(a). The peaks assigned to α-phase perovskite can be found in all films, but with significantly different content of remnant PbI_2 phase. In the case of DMSO-0% and DMSO-20%, a negligible PbI_2 peak demonstrates the almost complete conversion of PbI_2 into perovskite. Nevertheless, considering the high intensity of (003) peak of PbI_2 in the spectra of DMSO-5% and DMSO-10%, the PbI_2 content in these perovskite films is considerably high. The appropriate residual PbI_2 in perovskite is helpful in achieving high performance because of its passivation effect on perovskite layer or interface between perovskite and ETL.[31] Additionally, PbI_2 can induce the grain to grow and improve the quality of perovskite film.[32] However, too much remnant PbI_2 will be harmful to the stability of PSCs, which accelerates the degradation of perovskite layer.[33] Therefore, the facile manipulation of residual PbI_2 is significant for achieving the highly efficient and stable PSCs. As shown in Fig. 3(b), the photographs of perovskite film exposed to ambient environment for 1 week indicate that the stability of perovskite in the case of DMSO-5% is best, the appropriate remnant of PbI_2 and optimized perovskite surface (Figs. 2(e)–2(h)) would be the main reason. The optical property of perovskite filmis investigated by the UV-Vis absorption spectra. As shown in Fig. 3(c), perovskite film derived from DMSO-5% shows the best absorption, resulting from its densely packed grains.

Fig. 3. (a) XRD patterns of perovskite films derived from DMSO-0%, DMSO-5%, DMSO-10%, and DMSO-20% respectively, (b) photographs of perovskite films stored in ambient environment for 1 week, and (c) absorbance spectra of perovskite films derived from DMSO-0%, DMSO-5%, DMSO-10%, and DMSO-20% respectively.

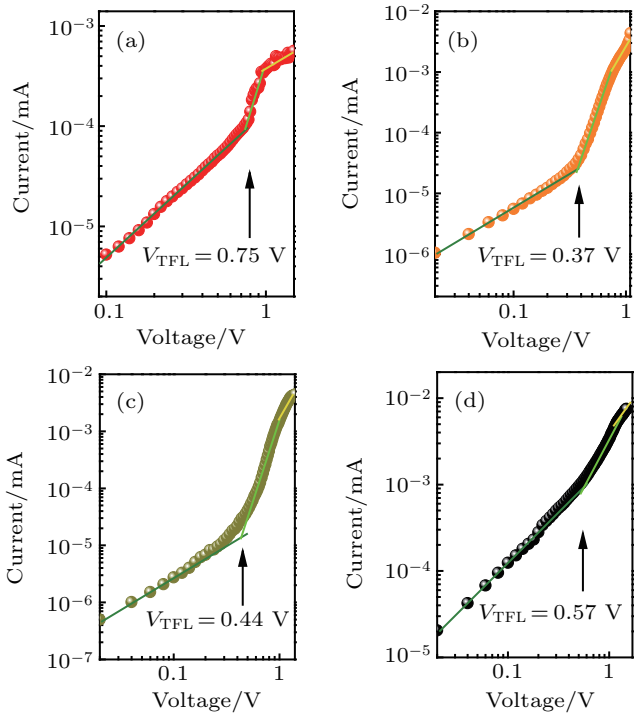

Fig. 4. Dark *I*–*V* curves of electron-only devices for perovskite films derived from (a) DMSO-0%, (b) DMSO-5%, (c) DMSO-10%, and (d) DMSO-20%, respectively.

For determining the trap densities of perovskite films, the dark *I*–*V* curves of electron-only devices are measured with configuration of ITO/SnO_2/perovskite/PCBM/Ag (Fig. A4), and the results are shown in Figs. 4(a)–4(d). All these curves display a distinct increase after the trap-filled limit voltage (V_{TFL}) has been reached, which can be used to calculate the trap density by the space-charge-limited-current (SCLC) technique from the following equation:

$$N_t = \frac{2\varepsilon\varepsilon_0 V_{TFL}}{eL^2},$$

in which e is the elementary charge, ε is the relative dielectric constant of perovskite (the ε of 46.9 is taken as the value of dielectric constant of $FAPbI_3$[12]), ε_0 is the vacuum permittivity, L denotes the thickness of perovskite layer, and N_t is the trap density of the perovskite film. The calculated trap densities are 4.57×10^{15} cm^{-3}, 2.25×10^{15} cm^{-3}, 2.68×10^{15} cm^{-3}, 3.47×10^{15} cm^{-3}, respectively. Apparently, the perovskite film derived from DMSO-5% shows the reduced level of trap density, which is consistent with the morphology and optical feature. It is beneficial to the improving of separation and transporting of charge carrier, as well as decreasing of trap recombination.

Not only does the quality of perovskite film play a crucial role in the operation of PSCs, but also the interfacial contact does. For investigating the contact between the perovskite layer and the PTAA layer, the AFM is employed to measure the roughness of perovskite films and the results are shown in Fig. A5. The roughness of films is consistent with the SEM results above, and the DMSO-5% perovskite film shows a smallest root mean square (RMS) value of about 28 nm. The charge carrier separation of PHJ PSC is located at the interface between perovskite and PTAA.[34] Therefore, the morphology of perovskite and interfacial contact between the perovskite layer and the PTAA layer play decisive roles in the photovoltaic performance of PSCs. Here in this work, the post-annealing of PbI_2 films has been a valid way to achieve high quality perovskite films and exquisite interfacial contact, which gives rise to the highly efficient separation and transport of light-induced charge carriers.

The photovoltaic performance parameters of PSCs are shown in Fig. 5 and Table 1. In the cases of DMSO-0%, DMSO-5%, and DMSO-10%, the fluctuation of PCE is mainly originated from the change of open circuit voltage (V_{oc}) and filling factor (FF). The PSCs prepared from DMSO-5% show the best average PCE of 18.08%, which benefits from the highest FF without sacrifice of V_{oc} and short circuit current density (J_{sc}). Meanwhile, they also show less deviation in average values as compared with other devices, which demonstrates the excellence reproducibility forDMSO-5% PSCs.

However, in the cases of DMSO-0% and DMSO-20% devices, the PCEs of devices diminish greatly and spread in a large range because of the decrease in V_{oc}, J_{sc}, and FF, as well as the bad stability. The loose contact of grains with many gaps and rough surface result in poor contact between perovskite layer and HTL, and induce the charge carriers to severely combine with each other or the current to leak during the operation of PSCs, which results in the performance deterioration. On the contrary, because of the lower trap density, smooth perovskite film, and exquisite interface contact between perovskite and PTAA, the PSC prepared from DMSO-5% shows the best efficiency, with a typical forward scanning PCE of 19.02% and an average FF of over 70% under 1-sun illumination, Additionally, as shown in Fig. 5(f), the stability of PSC using PTAA as the HTL is much better than conventional ones using Spiro-OMeTAD as the HTL, resulting from the hydrophobicity of PTAA and exquisite contact between perovskite layer and PTAA.

Table 1. Average photovoltaic performance parameters of PSCs derived from DMSO-0%, DMSO-5%, DMSO-10%, and DMSO-20%, respectively. Statistical data are based on 12 devices. The highest PCEs are shown in brackets.

	V_{oc}/V	J_{sc}/(mA/cm^2)	FF/%	PCE/%
DMSO-0%	1.01 ± 0.03	23.87 ± 0.42	60.5 ± 4.0	14.57 ± 1.39 (16.09)
DMSO-5%	1.05 ± 0.02	23.97 ± 0.58	72.0 ±0.7	18.08 ± 0.69 (19.02)
DMSO-10%	1.03 ± 0.03	23.38 ± 1.07	66.0 ±3.3	15.99 ± 1.23 (17.80)
DMSO-20%	0.83 ± 0.11	19.25 ± 4.12	56.6 ±4.7	9.36 ± 3.77 (13.39)

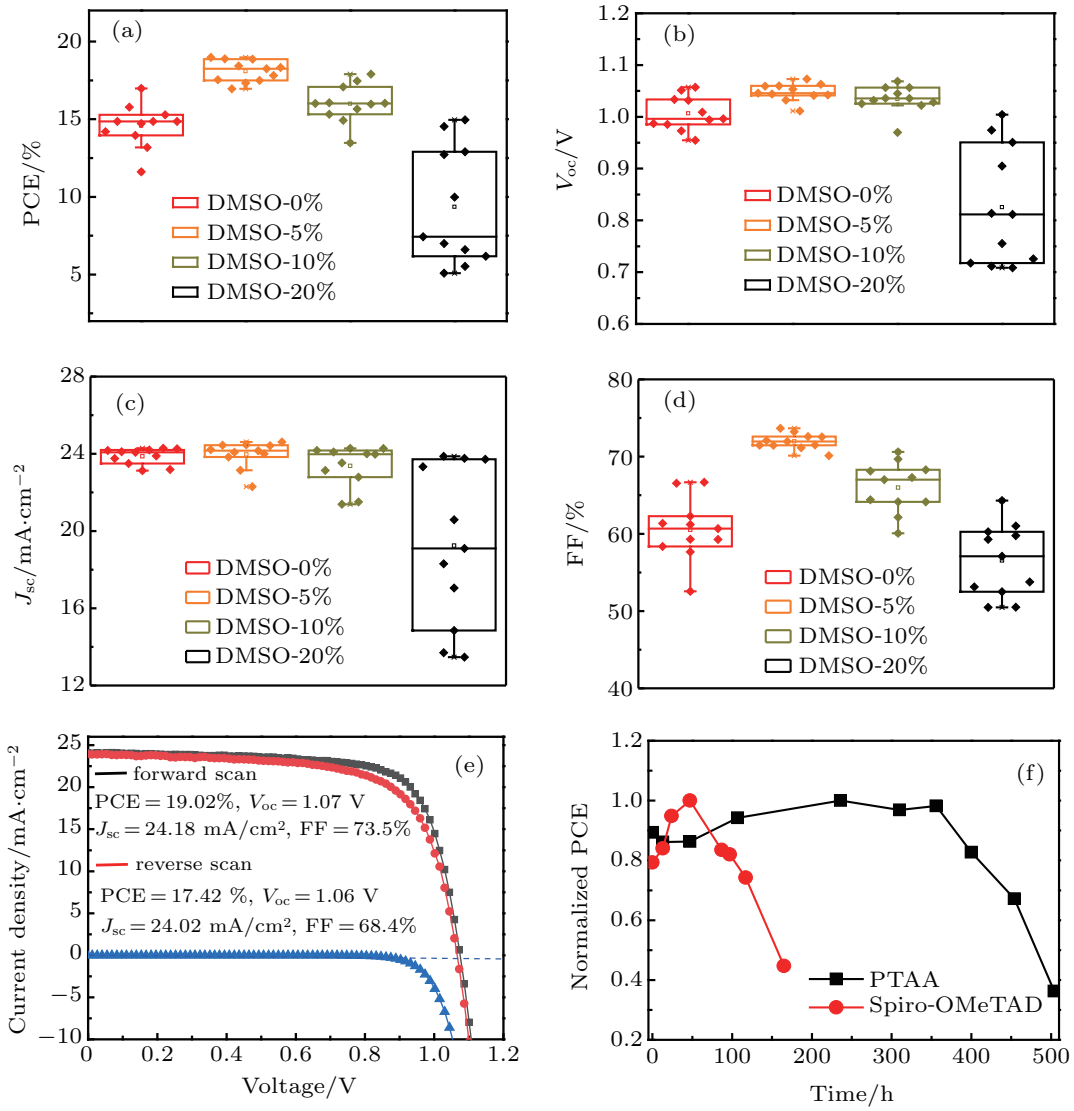

Fig. 5. (a)–(d) Photovoltaic performance parameters of PSCs derived from DMSO-0%, DMSO-5%, DMSO-10%, and DMSO-20%, respectively. (e) Typical current density-voltage curves of PSCs measured under simulated AM1.5 sunlight of 100 mW/cm^2. (f) Normalized PCE of PTAA and Spiro-OMeTAD-based PSCs, respectively.

4. Conclusions

By optimizing the ratio of DMSO to DMF in PbI_2 precursor, the morphology of PbI_2 film becomes controllable, which significantly affects the nucleation, growth and ripening process. A suitable crystallinity and morphology of PbI_2 film have a significant influence on the quality of subsequent perovskite film prepared by the two-step deposition. The dense, smooth and low-trap density perovskite films could be prepared by preparing high-quality PbI_2 substrate, which gives rise to the exquisite interface contact between perovskite and PTAA. The exquisite interface promotes the separation and transport of charge carriers, and thus boosting the PCE up 19.02%. A simple and facile modified two-step sequential deposition technique is developed by precisely adjusting the content of DMSO, which is believed to be helpful for the large-area fabrication of PSC.

Appendix A: Supporting information

The PbI_2(DMSO) complex content in precursor film is detected by SEM–EDS analysis. The results are shown in Figs. A1 and A2.

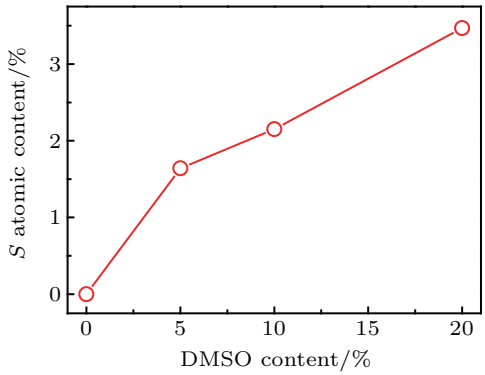

Fig. A1. *S* atomic content *versus* DMSO content in as-prepared PbI_2 precursor films detected by SEM–EDS.

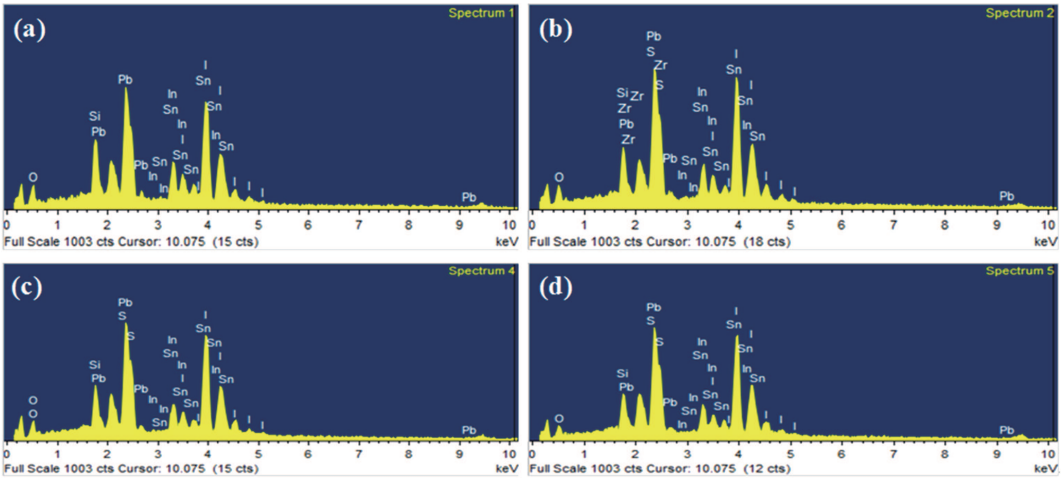

Fig. A2. SEM–EDS analysis of as-prepared PbI_2 films of (a) DMSO-0%, (b) DMSO-5%, (c) DMSO-10%, and (d) DMSO-20%.

The grain size in the perovskite films fabricated from DMSO-0%, DMSO-5%, DMSO-10%, and DMSO-20% PbI_2 films are shown in Fig. A3 and Table A1.

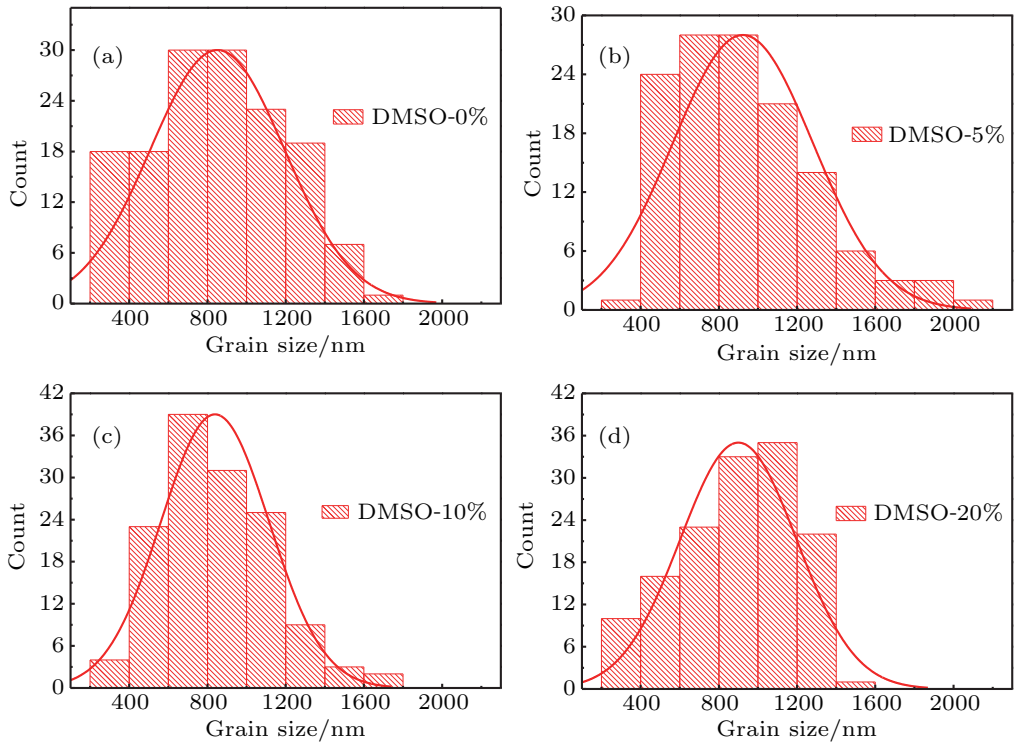

Fig. A3. Grain size distributions of perovskite films derived from (a) DMSO-0%, (b) DMSO-5%, (c) DMSO-10%, and (d) DMSO-20% PbI_2 films, respectively.

Table A1. Average grain size of different perovskite films.

MSS	DMSO-0%	DMSO-5%	DMSO-10%	DMSO-20%
Average grain size/nm	851	923	839	900

The architecture of electron-only device used for measuring trap density in perovskite film is shown in Fig. A4.

The AFM images for measuring the roughness of perovskite films are shown in Fig. A5

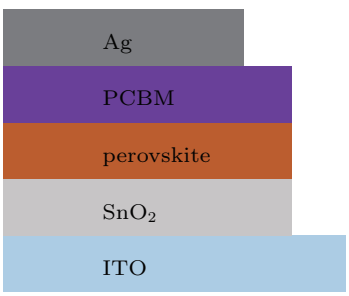

Fig. A4. Device architecture of electron-only device used for determining trap density in perovskite film.

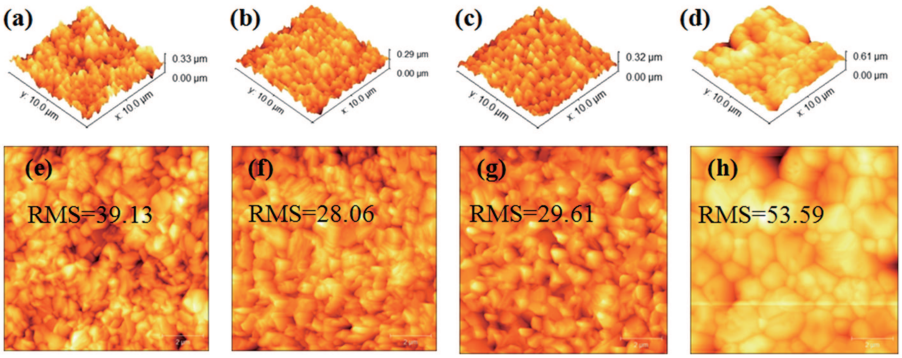

Fig. A5. AFM images of ((a)–(d)) 3D patterns and ((e)–(f)) surface morphologies for perovskite films derived from DMSO-0%, DMSO-5%, DMSO-10%, and DMSO-20%, respectively, with scanning area of 10 μm×10 μm, of which average RMS values are about 39 nm, 28 nm, 30 nm, and 54 nm, respectively.

References

[1] Gu Y F, Du H J, Li N N, Yang L and Zhou C Y 2019 *Chin. Phys. B* **28** 047101

[2] Liu B, Long M Q, Cai M Q and Yang J L 2018 *J. Phys. D: Appl. Phys.* **51** 105101

[3] Diao X F, Tang Y L and Xie Q 2019 *Chin. Phys. B* **28** 017802

[4] Wang C H, Zhang C J, Tong S C, Xia H Y, Wang L J, Xie H P, Gao Y L and Yang J L 2018 *J. Phys. D: Appl. Phys.* **51** 025110

[5] Chao L F, Xia Y D, Li B X, Xing G C, Chen Y H and Huang W 2019 *Chem.* **5** 995

[6] Hou Y, Du X Y, Scheiner S, McMeekin D P, Wang Z P, Li N, Killian M S, Chen H W, Richter M, Levchuk I, Schrenker N, Spiecker E, Stubhan T, Luechinger N A, Hirsch A, Schmuki P, Steinrück H P, Fink R H, Halik M, Snaith H J and Brabec C J 2017 *Science* **358** 1192

[7] *Best Research-Cell Efficiency Chart/Photovoltaic Research/NREL* October 2019

[8] Liu B, Long M Q, Cai M Q and Yang J L 2018 *Appl. Phys. Lett.* **112** 043901

[9] Heo J H, Im S H, Noh J H, Mandal T N, Lim C S, Chang J A, Lee Y H, Kim H J, Sarkar A, Nazeeurddin M K, Grätzel M and Seok S I 2013 *Nat. Photon.* **7** 486

[10] Yang W S, Park B W, Jung E H, Jeon N J, Kim Y C, Lee D U, Shin S S, Seo J, Kim E K, Noh J H and Seok S I 2017 *Science* **356** 1376

[11] Jeon N J, Noh J H, Kim Y C, Yang W S, Ryu S and Seok S I 2014 *Nat. Mater.* **13** 897

[12] Wu Y H, Wang P, Wang S B, Wang Z H, Cai B, Zheng X J, Chen Y, Yuan N Y, Ding J N and Zhang W H 2018 *ChemSusChem.* **11** 837

[13] Wu H, Zhang C J, Ding K X, Wang L J, Gao Y L and Yang J L 2017 *Org. Electron.* **45** 302

[14] Yang W S, Noh J H, Jeon N J, Kim Y C, Ryu S, Seo J and Seok S I 2015 *Science* **348** 1234

[15] Xu G Y, Xue R M, Chen W J, Zhang J W, Zhang M Y, Chen H Y, Cui C H, Li H K, Li Y W and Li Y F 2018 *Adv. Energy Mater.* **8** 1703054

[16] Huang K Q, Li H Y, Zhang Y X, Liu T J, Zhang J, Gao Y L, Peng Y Y, Ding L M and Yang J L 2019 *Sol. RRL* **3** 1800318

[17] Xiong J, Yang B C, Wu R S, Huang Y L, Sun J, Zhang J, Tao S H, Gao Y L and Yang J L 2016 *Org. Electron.* **30** 30

[18] Huang F Z, Pascoe A R, Wu W Q, Ku Z L, Peng Y, Zhong J, Caruso R A and Cheng Y B 2017 *Adv. Mater.* **29** 1601715

[19] Huang K Q, Wang C H, Zhang C J, Tong S C, Li H Y, Liu B, Gao Y X, Dong Y N, Gao Y L, Peng Y Y and Yang J L 2018 *Org. Electron.* **55** 140

[20] Qin P, Tetreault N, Dar M I, Gao P, McCall K L, Rutter S R, Ogier S D, Forrest N D, Bissett J S, Simms M J, Page A J, Fisher R, Grätzel M and Nazeeruddin M K 2015 *Adv. Energy Mater.* **5** 1400980

[21] Wu C G, Chiang C H, Tseng Z L, Nazeeruddin M K, Hagfeldt A and Grätzel M 2015 *Energy Environ. Sci.* **8** 2725

[22] Chiang C H and Wu C G 2016 *Nat. Photon.* **10** 196

[23] Liang P W, Liao C Y, Chueh C C, Zuo F, Spencer T, Xu K X, Lin J J and Alex J Y 2014 *Adv. Mater.* **26** 3748

[24] Eperon G E, Stranks S D, Menelaou C, Johnston M B, Herz L M and Snaith H J 2014 *Energy Environ. Sci.* **7** 982

[25] Yang L J, Wang J and Leung W W F 2015 *ACS Appl. Mater. Interfaces* **7** 14614

[26] Wu Y Z, Islam A, Yang X D, Qin C J, Liu J, Zhang K, Peng W Q and Han L Y 2014 *Energy Environ. Sci.* **7** 2934

[27] Jiang Q, Chu Z M, Wang P Y, Yang X L, Liu H, Wang Y, Yin Z G, Wu J L, Zhang X W and You J B 2017 *Adv. Mate.* **29** 1703852

[28] Yang W S, Noh J H, Jeon N J, Kim Y C, Ryu S, Seo J and Seok S I 2015 *Science* **348** 1234

[29] Wakamiya A, Endo M, Sasamori T, Tokitoh N, Ogomi Y, Hayase S Z and Murata Y 2014 *Chem. Lett.* **43** 711

[30] Yi C Y, Li X, Luo J S, Zakeeruddin S M and Grätzel M 2016 *Adv. Mater.* **28** 2964

[31] Peng Y Y, Cheng Y D, Wang C H, Zhang C J, Xia H Y, Huang K Q, Tong S C, Hao X T and Yang J L 2018 *Org. Electron.* **58** 153

[32] Chen Q, Zhou H P, Song T B , Luo S, Hong Z R, Duan H S , Dou L T, Liu Y S and Yang Y 2014 *Nano Lett.* **14** 4158

[33] Jacobsson T J, Correa-Baena J P, Anaraki E H, Philippe B, Stranks S D, Bouduban M E F, Tress W, Schenk K, Teuscher J, Moser J E, Rensmo H and Hagfeldt A 2016 *J. Am. Chem. Soc.* **138** 10331

[34] Cai M L, Ishida N, Li X, Yang X D, Noda T, Wu Y Z, Xie F X, Naito H, Fujita D and Han L Y 2018 *Joule* **2** 296